

Search for direct CP violating charge asymmetries in $K^\pm \rightarrow \pi^\pm \pi^+ \pi^-$ and $K^\pm \rightarrow \pi^\pm \pi^0 \pi^0$ decays

The NA48/2 Collaboration

J.R. Batley, A.J. Culling, G. Kalmus, C. Lazzeroni, D.J. Munday, M.W. Slater,
S.A. Wotton

*Cavendish Laboratory, University of Cambridge, Cambridge, CB3 0HE, U.K.*¹

R. Arcidiacono, G. Bocquet, N. Cabibbo, A. Ceccucci, D. Cundy², V. Falaleev,
M. Fidecaro, L. Gatignon, A. Gonidec, W. Kubischta, A. Norton, A. Maier, M. Patel,
A. Peters

CERN, CH-1211 Genève 23, Switzerland

S. Balev, P.L. Frabetti, E. Goudzovski³, P. Hristov⁴, V. Kekelidze, V. Kozhuharov,
L. Litov, D. Madigozhin, E. Marinova, N. Molokanova, I. Polenkevich, Yu. Potrebenikov,
S. Stoynev, A. Zinchenko

Joint Institute for Nuclear Research, 141980 Dubna, Russian Federation

E. Monnier⁵, E. Swallow, R. Winston

The Enrico Fermi Institute, The University of Chicago, Chicago, Illinois, 60126, U.S.A.

P. Rubin, A. Walker

*Department of Physics and Astronomy, University of Edinburgh, JCMB King's Buildings,
Mayfield Road, Edinburgh, EH9 3JZ, U.K.*

W. Baldini, A. Cotta Ramusino, P. Dalpiaz, C. Damiani, M. Fiorini, A. Gianoli,
M. Martini, F. Petrucci, M. Savrié, M. Scarpa, H. Wahl

Dipartimento di Fisica dell'Università e Sezione dell'INFN di Ferrara, I-44100 Ferrara, Italy

A. Bizzeti⁶, M. Calvetti, E. Celeghini, E. Iacopini, M. Lenti, F. Martelli⁷,
G. Ruggiero³, M. Veltri⁷

Dipartimento di Fisica dell'Università e Sezione dell'INFN di Firenze, I-50125 Firenze, Italy

M. Behler, K. Eppard, K. Kleinknecht, P. Marouelli, L. Masetti⁸, U. Moosbrugger,
C. Morales Morales, B. Renk, M. Wache, R. Wanke, A. Winhart

*Institut für Physik, Universität Mainz, D-55099 Mainz, Germany*⁹

D. Coward¹⁰, A. Dabrowski, T. Fonseca Martin⁴, M. Shieh, M. Szleper, M. Velasco,
M.D. Wood¹¹

*Department of Physics and Astronomy, Northwestern University, Evanston Illinois
60208-3112, U.S.A.*

G. Anzivino, P. Cenci, E. Imbergamo, A. Nappi, M. Pepe, M.C. Petrucci, M. Piccini,
M. Raggi, M. Valdata-Nappi

Dipartimento di Fisica dell'Università e Sezione dell'INFN di Perugia, I-06100 Perugia, Italy

C. Cerri, G. Collazuol, F. Costantini, L. DiLella, N. Doble, R. Fantechi, L. Fiorini,
S. Giudici, G. Lamanna, I. Mannelli, A. Michetti, G. Pierazzini, M. Sozzi

*Dipartimento di Fisica dell'Università, Scuola Normale Superiore e Sezione dell'INFN di Pisa,
I-56100 Pisa, Italy*

B. Bloch-Devaux, C. Cheshkov⁴, J.B. Chèze, M. De Beer, J. Derré, G. Marel,
E. Mazzucato, B. Peyaud, B. Vallage
DSM/DAPNIA - CEA Saclay, F-91191 Gif-sur-Yvette, France

M. Holder, M. Ziolkowski
*Fachbereich Physik, Universität Siegen, D-57068 Siegen, Germany*¹²

S. Bifani, C. Biino, N. Cartiglia, M. Clemencic⁴, S. Goy Lopez, F. Marchetto
*Dipartimento di Fisica Sperimentale dell'Università e Sezione dell'INFN di Torino, I-10125
Torino, Italy*

H. Dibon, M. Jeitler, M. Markytan, I. Mikulec, G. Neuhofer, L. Widhalm
*Österreichische Akademie der Wissenschaften, Institut für Hochenergiephysik, A-10560 Wien,
Austria*¹³

To be submitted to European Physics Journal C.

Abstract

A measurement of the direct CP violating charge asymmetries of the Dalitz plot linear slopes $A_g = (g^+ - g^-)/(g^+ + g^-)$ in $K^\pm \rightarrow \pi^\pm \pi^+ \pi^-$ and $K^\pm \rightarrow \pi^\pm \pi^0 \pi^0$ decays by the NA48/2 experiment at CERN SPS is presented. A new technique of asymmetry measurement involving simultaneous K^+ and K^- beams and a large data sample collected allowed a result of an unprecedented precision. The charge asymmetries were measured to be $A_g^c = (-1.5 \pm 2.2) \times 10^{-4}$ with 3.11×10^9 $K^\pm \rightarrow \pi^\pm \pi^+ \pi^-$ decays, and $A_g^n = (1.8 \pm 1.8) \times 10^{-4}$ with 9.13×10^7 $K^\pm \rightarrow \pi^\pm \pi^0 \pi^0$ decays. The precision of the results is limited mainly by the size of the data sample.

¹Funded by the U.K. Particle Physics and Astronomy Research Council

²Present address: Istituto di Cosmogeofisica del CNR di Torino, I-10133 Torino, Italy

³Present address: Scuola Normale Superiore and INFN, I-56100 Pisa, Italy

⁴Present address: CERN, CH-1211 Genève 23, Switzerland

⁵Also at Centre de Physique des Particules de Marseille, IN2P3-CNRS, Université de la Méditerranée, Marseille, France

⁶Also Istituto di Fisica, Università di Modena, I-41100 Modena, Italy

⁷Istituto di Fisica, Università di Urbino, I-61029 Urbino, Italy

⁸Present address: Physikalisches Institut, Universität Bonn, D-53115 Bonn, Germany

⁹Funded by the German Federal Minister for Education and research under contract 05HK1UM1/1

¹⁰Permanent address: SLAC, Stanford University, Menlo Park, CA 94025, U.S.A.

¹¹Present address: UCLA, Los Angeles, CA 90024, U.S.A.

¹²Funded by the German Federal Minister for Research and Technology (BMBF) under contract 056SI74

¹³Funded by the Austrian Ministry for Traffic and Research under the contract GZ 616.360/2-IV GZ 616.363/2-VIII, and by the Fonds für Wissenschaft und Forschung FWF Nr. P08929-PHY

Introduction

For more than 20 years, after the discovery in 1964 that the long lived neutral kaon could decay to the same 2π final state as the short lived one [1], demonstrating that the mass eigenstates of the neutral kaons consist of a mixture of even and odd eigenstates under the combined operation of Charge conjugation and Parity, no other manifestation of CP violation was detected despite intensive experimental investigation. In the meanwhile the discovery of the three families of quarks and the development of the Standard Model (SM) made it plausible that CP violation was in fact a general property of the weak interactions, originating from a single non-trivial phase in the CKM matrix of the coefficients involved in flavour changing transitions. It was in particular realized that, barring accidental cancellations, CP violation should be relevant not only in meson-antimeson mixing but also in decays (direct CP violation) and in so called mixing induced transitions.

Two major experimental breakthroughs have since taken place. In the late 1990s, following an earlier indication by NA31 [2], the NA48 and KTeV experiments firmly established the existence of direct CP violation [3, 4] by measuring a non-zero value of the parameter $\text{Re}(\varepsilon'/\varepsilon)$ parameter in $K^0 \rightarrow 2\pi$ decays. More recently the B-factory experiments Babar and Belle discovered a series of CP violating effects in the system of the neutral B meson [5, 6].

In order to explore possible non-SM enhancements to heavy-quark loops, which are at the core of direct CP-violating processes, all possible manifestations of direct CP violation have to be studied experimentally. In kaon physics, besides the already investigated parameter $\text{Re}(\varepsilon'/\varepsilon)$, the most promising complementary observables are the rates of GIM-suppressed flavour-changing neutral current decays $K \rightarrow \pi\nu\bar{\nu}$, and the charge asymmetry between K^+ and K^- decays into 3π .

It is difficult to constrain the fundamental parameters of the theory using measurements of direct CP violation in decay amplitudes due to the presence of non-perturbative hadron effects. Still, an intense theoretical programme is under way to improve predictions, aiming to allow the direct CP violation measurements to be used as quantitative constraints on the SM.

The $K^\pm \rightarrow 3\pi$ matrix element squared is conventionally parameterized [7] by a polynomial expansion¹

$$|M(u, v)|^2 \sim 1 + gu + hu^2 + kv^2, \quad (1)$$

where g, h, k are the so called linear and quadratic Dalitz plot slope parameters ($|h|, |k| \ll |g|$), and the two Lorentz invariant kinematic variables u and v are defined as

$$u = \frac{s_3 - s_0}{m_\pi^2}, \quad v = \frac{s_2 - s_1}{m_\pi^2}, \quad s_i = (P_K - P_i)^2, \quad i = 1, 2, 3; \quad s_0 = \frac{s_1 + s_2 + s_3}{3}. \quad (2)$$

Here m_π is the charged pion mass, P_K and P_i are the kaon and pion four-momenta, the indices $i = 1, 2$ correspond to the two pions of the same electrical charge (“even” pions, so that v is defined up to a sign), and the index $i = 3$ to the pion of different charge (the “odd” pion). A difference between the slope parameters g^+ and g^- describing the decays

¹At the next order of approximation, electromagnetic interactions and final state $\pi\pi$ rescattering should be included into the decay amplitude [8, 9, 10]. These effects, despite being charge-symmetric, may still contribute to the interpretation of the results, as will be discussed below.

47 of positive and negative kaons, respectively, is a manifestation of direct CP violation
 48 usually expressed by the corresponding slope asymmetry

$$A_g = (g^+ - g^-)/(g^+ + g^-) \approx \Delta g/(2g), \quad (3)$$

49 where Δg is the slope difference and g is the average linear slope. In general terms, the
 50 slope asymmetry is expected to be strongly enhanced with respect to the asymmetry of
 51 integrated decay rates [11]. A recent full next-to-leading order ChPT computation [12]
 52 predicts A_g to be of the order of 10^{-5} within the SM. Another SM calculation [13] predicts
 53 the asymmetry in the $K^\pm \rightarrow \pi^\pm \pi^0 \pi^0$ decay to be of the order of 10^{-6} (in agreement
 54 with [12] within the errors). Theoretical calculations involving processes beyond the
 55 SM [14] allow a wider range of A_g , including substantial enhancements up to a few 10^{-4} .

56 In the past years, several experiments have searched for the CP violating slope asym-
 57 metry in both $\pi^\pm \pi^+ \pi^-$ and $\pi^\pm \pi^0 \pi^0$ decay modes by collecting samples of K^+ and K^-
 58 decays [15, 16]. These measurements set upper limits on A_g at the level of a few 10^{-3} ,
 59 limited by systematic uncertainties.

60 The primary goal of the NA48/2 experiment at the CERN SPS is the measurement
 61 of the slope charge asymmetries A_g in both $K^\pm \rightarrow \pi^\pm \pi^+ \pi^-$ and $K^\pm \rightarrow \pi^\pm \pi^0 \pi^0$ processes
 62 with a sensitivity at least one order of magnitude better than previous experiments.
 63 The new level of precision can explore effects, albeit larger than the SM predictions,
 64 induced by new physics, and is achieved by using a novel measurement technique based
 65 on simultaneous K^+ and K^- beams overlapping in space.

66 Measurements of A_g in both decay modes, performed with approximately half of the
 67 NA48/2 data sample have been published [17, 18]. This paper presents the final results,
 68 superseding these earlier results.

69 The plan of the paper is the following. In Section 1 the experimental setup is described.
 70 Section 2 contains the description of the method developed for the measurement of the
 71 slope difference which is common to both decay modes, and which aims to cancel first
 72 order systematic biases. The analyses of the $K^\pm \rightarrow \pi^\pm \pi^+ \pi^-$ and $K^\pm \rightarrow \pi^\pm \pi^0 \pi^0$ decay
 73 modes are discussed in Sections 3 and 4, respectively. Discussion of the results follows in
 74 Section 5.

75 1 Beams and detectors

76 1.1 Simultaneous K^+ and K^- beams

77 A high precision measurement of A_g (at the level of 10^{-4}) requires a dedicated experi-
 78 mental approach together with collection of very large data samples. A novel beam line
 79 providing for the first time two simultaneous charged beams of opposite signs superim-
 80 posed in space over the decay fiducial volume was designed and built in the high intensity
 81 hall (ECN3) at the CERN SPS. The beam line is a key element of the experiment, as
 82 it allows decays of K^+ and K^- to be recorded at the same time, and therefore leads to
 83 cancellation of several systematic uncertainties for the charge asymmetry measurement.
 84 Regular alternation of magnetic fields in all the beam line elements was adopted, which
 85 contributed to symmetrization of the average geometrical acceptance for K^+ and K^-
 86 decays. The layout of the beams and detectors is shown schematically in Fig. 1.

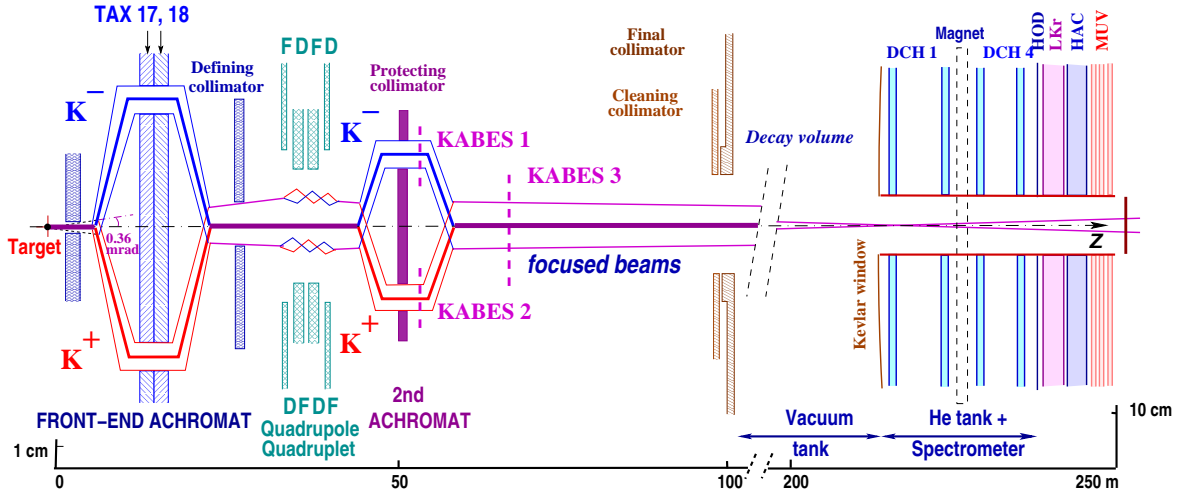


Figure 1: Schematic side view of the NA48/2 beam line (TAX17,18: motorized beam dump/collimators used to select the momentum of the K^+ and K^- beams, FDFD/DFDF: focusing quadrupoles, KABES1–3: kaon beam spectrometer stations), decay volume and detector (DCH1–4: drift chambers, HOD: hodoscope, LKr: EM calorimeter, HAC: hadron calorimeter, MUV: muon veto). Thick lines indicate beam axes, narrow ones the projection of their envelopes. Note that the vertical scales are different in the two parts of the figure.

87 The setup is described in a right-handed orthogonal coordinate system with the z
 88 axis directed downstream along the beam, and the y axis directed vertically up. Thus
 89 the horizontal x coordinate is such that the negative (positive) x point to the Salève
 90 (Jura) mountains. The Salève/Jura notation is used in the following analysis to denote
 91 the spectrometer magnet polarity.

92 The beams are produced by 400 GeV/ c protons (delivered from the CERN SPS with
 93 a duty cycle of 4.8 s/16.8 s) impinging on a beryllium target of 40 cm length and 2 mm
 94 diameter. Both beams leave the target on axis at zero production angle, thereby ensuring
 95 that their source is geometrically similar and that the K^+/K^- flux ratio remains stable.
 96 It was demonstrated that the small residual difference of K^+ and K^- momentum spectra
 97 produces a negligible effect on the measurement. Charged particles with momenta (60 ± 3)
 98 GeV/ c are selected in a charge-symmetric way by an achromatic system of four dipole
 99 magnets with zero total deflection (‘achromat’), which splits the two beams in the vertical
 100 plane and then recombines them on a common axis. Then the beams pass through a
 101 defining collimator and a series of four quadrupoles designed to produce horizontal and
 102 vertical charge-symmetric focusing of the beams towards the detector. Finally the two
 103 beams are again split in the vertical plane and recombined by a second achromat, where
 104 three stations of a Micromegas-type [19] detector operating in TPC mode form a kaon
 105 beam spectrometer KABES [20] (not used in the present analyses).

106 After passing through the cleaning and final collimators, the beams enter the decay
 107 volume housed in a 114 m long cylindrical vacuum tank with a diameter of 1.92 m for
 108 the first 65 m, and 2.4 m for the rest. Both beams follow the same path in the decay
 109 volume: their axes coincide to 1 mm, while their lateral sizes are about 1 cm. With
 110 7×10^{11} protons per burst incident on the target, the positive (negative) beam flux at
 111 the entrance of the decay volume is 3.8×10^7 (2.5×10^7) particles per pulse (primarily

112 charged pions), of which 5.7% (4.9%) are K^+ (K^-). The K^+/K^- flux ratio is about 1.8
 113 and stable to within 1%; no correlations were observed between its variation in time and
 114 time-dependent inefficiencies of the setup. The fraction of beam kaons decaying in the
 115 decay volume at nominal momentum is 22%.

116 1.2 Main detectors

117 The decay volume is followed by a magnetic spectrometer [21] used to reconstruct tracks
 118 of charged particles. The spectrometer is housed in a tank filled with helium at nearly
 119 atmospheric pressure, separated from the vacuum tank by a thin ($0.31\%X_0$) Kevlar com-
 120 posite window. A thin-walled aluminium beam pipe of 16 cm outer diameter travers-
 121 ing the centre of the spectrometer and all the following detectors allows the undecayed
 122 beam particles and the muon halo from decays of beam pions to continue their path
 123 in vacuum. The spectrometer consists of four identical drift chambers (DCH): DCH1,
 124 DCH2 located upstream, and DCH3, DCH4 downstream of a dipole magnet. The magnet
 125 has a field integral $\int B_y dz = 0.4$ Tm, providing a horizontal transverse momentum kick
 126 $\Delta P_x = 120$ MeV/ c for charged particles. The DCHs have the shape of a regular octagon
 127 with transverse size of about 2.8 m and fiducial area of about 4.5 m². Each chamber is
 128 composed of eight planes of sense wires arranged in four pairs of staggered planes oriented
 129 horizontally, vertically, and along each of the two orthogonal 45° directions. The spatial
 130 resolution of each DCH is $\sigma_x = \sigma_y = 90$ μ m. The nominal momentum resolution of the
 131 magnetic spectrometer is $\sigma_p/p = (1.02 \oplus 0.044 \cdot p)\%$ (p expressed in GeV/ c). The mea-
 132 sured resolution on the reconstructed $3\pi^\pm$ invariant mass varied during the data taking
 133 time in the range of $(1.65 - 1.72)$ MeV/ c^2 in 2003 data, and $(1.76 - 1.82)$ MeV/ c^2 in
 134 2004, depending on DCH performance (generally, the chambers were operated at lower
 135 high voltage in 2004).

136 The magnetic spectrometer is followed by a plastic scintillator hodoscope (HOD) used
 137 to produce fast trigger signals and to provide precise time measurements of charged parti-
 138 cles. The HOD, with a transverse size of about 2.4 m, consists of a plane of vertical and a
 139 plane of horizontal strip-shaped counters, each plane comprising 64 counters arranged in
 140 four quadrants. Each quadrant is logically subdivided into 4 subquadrants (“segments”)
 141 which take part in the trigger logic. Counter widths (lengths) vary from 6.5 cm (121 cm)
 142 for central counters to 9.9 cm (60 cm) for peripheral ones.

143 The HOD is followed by a liquid krypton electromagnetic calorimeter (LKr) [22] used
 144 to detect electrons and photons. It is an almost homogeneous ionization chamber with
 145 an active volume of 7 m³ of liquid krypton, segmented transversally into 13248 projective
 146 cells, 2×2 cm² each, by a system of Cu–Be ribbon electrodes, and with no longitudinal
 147 segmentation. The calorimeter is $27X_0$ deep and has an energy resolution $\sigma(E)/E =$
 148 $0.032/\sqrt{E} \oplus 0.09/E \oplus 0.0042$ (E is expressed in GeV). The spatial resolution for a single
 149 electromagnetic shower is $\sigma_x = \sigma_y = 0.42/\sqrt{E} \oplus 0.06$ cm for the transverse coordinates x
 150 and y .

151 The LKr is followed by a hadronic calorimeter (HAC) and a muon detector (MUV),
 152 both not used in the present analyses. A detailed description of the components of the
 153 NA48 detector can be found elsewhere [23].

1.3 Trigger logic

The event rate of ~ 500 kHz is dominated by $K^\pm \rightarrow \mu^\pm \nu$ and $K^\pm \rightarrow \pi^\pm \pi^0$ decays, which are of limited physics interest as such within the NA48/2 programme. A two-level trigger system is used to select the $K^\pm \rightarrow 3\pi$ decay modes for readout, reducing the event rate to ~ 10 kHz.

At the first level (L1), the $K^\pm \rightarrow \pi^\pm \pi^+ \pi^-$ decays are triggered by requiring coincidences of hits in the two HOD planes in at least two of the 16 segments (the L1C condition). The $K^\pm \rightarrow \pi^\pm \pi^0 \pi^0$ decays are triggered by requiring a coincidence of the two HOD planes in at least one segment, and the presence of at least two distinguishable clusters of energy deposition in the LKr (the L1N condition). In some periods of data taking the L1N condition also used as input the total LKr energy deposition (see Section 4.4). The L1C signal is produced by the HOD logic, while the L1N signal consists of HOD and LKr components. These two components require separate analyses in order to study possible biases to the asymmetry measurement.

The second level trigger (L2) is based on a real time system computing coordinates of DCH hits using DCH drift times, and a farm of asynchronous microprocessors performing a fast reconstruction of tracks and running a decision-taking algorithm.

The L2 algorithm selecting the $K^\pm \rightarrow \pi^\pm \pi^0 \pi^0$ events (L2N) examines the events passing the L1N condition, and requires the existence of a reconstructed track which, assumed to be a pion, has an energy $E^* < 230$ MeV in the rest frame of a K^\pm having a momentum of 60 GeV/ c directed along the z axis. This condition suppresses the $K^\pm \rightarrow \pi^\pm \pi^0$ decays (which have $E^* = 248$ MeV), while keeping the $K^\pm \rightarrow \pi^\pm \pi^0 \pi^0$ decays (for which E^* ranges between 140 MeV and 193 MeV).

The L2 algorithm selecting the $K^\pm \rightarrow \pi^\pm \pi^+ \pi^-$ events (L2C) examines the events passing the L1C condition, and requires at least two tracks to originate in the decay volume with the reconstructed distance of closest approach below 5 cm. L1C triggers not satisfying this condition are examined further and accepted if the L2N condition is satisfied.

NA48/2 collected data during two runs in 2003 and 2004, with ~ 50 days of efficient data taking in each run. About 18×10^9 triggers, and 200 TB of data were recorded in total.

2 The method of the slope difference measurement

2.1 Data taking strategy

Charge symmetrization of the experimental conditions is to a large extent achieved by using simultaneous superimposed K^+ and K^- beams with similar momentum spectra. However, the presence of magnetic fields in both the beam line (achromats, focusing quadrupoles, etc.) and the magnetic spectrometer, combined with some asymmetries in detector performance, introduces residual charge asymmetries. In order to equalize the local effects on the acceptance, the polarities of all the magnets in the beam transport system were reversed during the data taking on an approximately weekly basis (corresponding to the periodicity of SPS technical stops), while the polarity of the spectrometer magnet was alternated on a more frequent basis (approximately once per day in 2003 and once every 3 hours in 2004).

196 Data collected over a period which has all four possible setup configurations (i.e.
 197 combinations of beam line and spectrometer magnet polarities), spanning about two weeks
 198 of efficient data taking, represent a “supersample” and is treated as an independent and
 199 self-consistent set of data for the asymmetry measurement.

200 For the $K^\pm \rightarrow \pi^\pm \pi^+ \pi^-$ analysis, nine supersamples numbered 0 to 8 were collected
 201 in two years of data taking (supersamples 0–3 in 2003 and supersamples 4–8 in 2004).
 202 For the $K^\pm \rightarrow \pi^\pm \pi^0 \pi^0$ analysis, a fraction of the data sample was rejected due to poor
 203 trigger performance, and another fraction of data was merged into a larger supersample to
 204 improve the balance of magnet polarities, which resulted in seven supersamples numbered
 205 I to VII (supersamples I–III in 2003 and supersamples IV–VII in 2004).

206 2.2 Fitting procedure

207 The u -projection of the Dalitz plot is sufficient to extract the information about Δg at
 208 the desired level of precision. The measurement method is based on comparing the recon-
 209 structed u -spectra of K^+ and K^- decays (denoted as $N^+(u)$ and $N^-(u)$, respectively).
 210 In the framework of the parameterization (1), the ratio $R(u) = N^+(u)/N^-(u)$ is in good
 211 approximation proportional to

$$R(u) \sim 1 + \frac{\Delta g u}{1 + gu + hu^2}, \quad (4)$$

212 the contribution of the kv^2 term integrated over v being negligible. The slope difference
 213 Δg can be extracted from a fit to $R(u)$ involving the measured slope parameters g and
 214 h [7, 24], and A_g can be evaluated as in Eq. (3).

215 The parameters describing the Dalitz plot distribution explicitly appear in the fitting
 216 function. This generates a certain dependence of the results on the assumed shape of the
 217 event density, which in our case is Eq. (1). These effects will be discussed later.

218 2.3 Cancellation of systematic effects

219 It should be noted that any instrumental effect can induce a fake slope difference only if
 220 it is: (1) charge asymmetric and (2) correlated with u .

221 For a given decay mode, each supersample contains four sets of simultaneously col-
 222 lected $K^+ \rightarrow 3\pi$ and $K^- \rightarrow 3\pi$ samples corresponding to the four different setup con-
 223 figurations (eight data samples in total). To measure the charge asymmetry, exploiting
 224 the cancellations of systematic biases emerging due to polarity reversals, the following
 225 “quadruple ratio” $R_4(u)$ is evaluated. It involves the eight corresponding u spectra, and
 226 is formed by the product of four $R(u) = N^+(u)/N^-(u)$ ratios with opposite kaon sign
 227 and a deliberately chosen setup configuration in numerator and denominator:

$$R_4(u) = R_{US}(u) \cdot R_{UJ}(u) \cdot R_{DS}(u) \cdot R_{DJ}(u). \quad (5)$$

228 Here the indices U/D denote beam line polarities corresponding to K^+ passing along the
 229 upper/lower path in the achromats of the beamline, while the indices S/J denote spec-
 230 trometer magnet polarities (opposite for K^+ and K^-) corresponding to the “even” (i.e.
 231 the two identical) pions from a $K^\pm \rightarrow \pi^\pm \pi^+ \pi^-$ decay being deflected to negative/positive
 232 x (i.e. towards the Salève/Jura mountains). For example, $R_{US}(u)$ is the ratio of the u

233 distribution for K^+ transported along the upper path in the beamline achromats and
 234 collected with a certain polarity of the spectrometer magnetic field, to the distribution for
 235 K^- transported along the lower path and collected with the opposite analyzing magnet
 236 polarity. A fit of the quadruple ratio (5) with a function of the form

$$f(u) = n \cdot \left(1 + \frac{\Delta g u}{1 + gu + hu^2} \right)^4 \quad (6)$$

237 results in the determination of two parameters: the normalization n and the difference of
 238 slopes Δg . The normalization is sensitive to the K^+/K^- flux ratio, while Δg is not.

239 The rationale for choosing the four ratios $R(u)$ appearing in (5) as the basic ones
 240 (which is not the only possibility) lies in the fact that they intrinsically cancel at first
 241 order instrumental effects linked to the imperfect left-right symmetry of the apparatus. As
 242 will be seen below, time variation of the left-right asymmetry (which is primarily due to
 243 variations of spectrometer misalignment and beam geometry) is the largest instrumental
 244 effect, and has been the primary subject of the analysis.

245 The quadruple ratio technique logically completes the procedure of magnet polarity
 246 reversal, and allows a three-fold cancellation of systematic biases in the data, without the
 247 need to rely on an accurate simulation of the instrumental asymmetries:

- 248 • due to spectrometer magnet polarity reversal, local detector inefficiencies cancel
 249 between K^+ and K^- samples with decay products reaching the same parts of the
 250 detector in each of the four ratios $R(u)$ appearing in the quadruple ratio $R_4(u)$;
- 251 • due to the simultaneous beams, global time-variable biases cancel between K^+ and
 252 K^- samples recorded at the same time in the product of $R_S(u)$ and $R_J(u)$ ratios;
- 253 • due to beam line polarity reversal, local beam line biases, resulting in slight differ-
 254 ences in beam profiles and momentum spectra, largely cancel between the $R_U(u)$
 255 and $R_D(u)$ ratios.

256 The method is independent of the K^+/K^- flux ratio and the relative sizes of the
 257 samples collected with different setup configurations. However, the statistical precision is
 258 limited mainly by the smallest of the samples involved, therefore the balance of sample
 259 sizes was controlled during the data taking. The result remains sensitive only to time
 260 variations of asymmetries in the experimental conditions which have a characteristic time
 261 smaller than the corresponding field alternation period.

262 2.4 Control quantities

263 In order to demonstrate that the level of cancellation of the systematic uncertainties
 264 achieved using the quadruple ratio technique is sufficient, the quantities cancelling in
 265 (5) have to be measured. For this purpose, slopes of two other control quadruple ratios
 266 built out of the eight u spectra are evaluated. These control ratios can be written as the
 267 products of the four ratios of the u spectra for same sign kaons recorded with different
 268 setup configurations. As a result, any physical asymmetry cancels in these ratios, while
 269 the setup asymmetries do not.

270 The fake slope difference Δg_{SJ} introduced by global time-dependent detector varia-
 271 tions does not cancel in a ratio with opposite spectrometer polarities and identical beam
 272 line polarities in numerator and denominator, or equivalently, in the adopted notation

$$R_{SJ}(u) = (R_{US}(u) \cdot R_{DS}(u)) / (R_{UJ}(u) \cdot R_{DJ}(u)). \quad (7)$$

273 Similarly, the fake slope difference Δg_{UD} introduced by the differences of the two beam
 274 paths does not cancel in a ratio with opposite beam line polarities and identical spec-
 275 trometer polarities, namely:

$$R_{UD}(u) = (R_{US}(u) \cdot R_{UJ}(u)) / (R_{DS}(u) \cdot R_{DJ}(u)). \quad (8)$$

276 It should be noted that time stability of the beam line conditions is much better than the
 277 (itself small) difference between the upper and lower beam paths.

278 The intrinsic left-right asymmetry of the experimental apparatus which, as already
 279 mentioned, cancels in each of the basic ratios appearing in (5), can not be directly mea-
 280 sured by the above two control ratios (although it is accessible within an analysis based
 281 in different choice of the basic ratios). These asymmetric effects, being the largest of the
 282 residual effects and the central subject of investigation, have been taken into account with
 283 dedicated methods (see Sections 3.2, 3.4).

284 Any possible systematic bias remaining in (5) is of a higher order effect than Δg_{SJ}
 285 and Δg_{UD} . Thus, a measurement of fake slope differences compatible with zero, within
 286 their statistical uncertainties, validates the measurement method.

287 2.5 Averaging over the independent data sets

288 As described in Section 2.1, the data sample is divided into several independent self-
 289 contained supersamples. Two methods of averaging the independent results over the
 290 supersamples were considered:

- 291 • averaging the measured quadruple ratios (5) independently for each u bin, and then
 292 fitting the resulting grand quadruple ratio with the function (6);
- 293 • independent fitting of the quadruple ratios in every supersample, and then averaging
 294 the results on Δg .

295 The first method allows the results to be presented in a compact form, i.e. in terms
 296 of a single spectrum for each of the two decay modes. On the other hand, the second
 297 method allows a cross-check concerning several aspects of the analysis, in particular the
 298 time stability of the results.

299 As will be demonstrated below, the two methods lead to similar results due to the
 300 good balance of statistics which was maintained between the supersamples.

301 2.6 Monte Carlo simulation

302 Due to the method described above, no Monte Carlo (MC) corrections to the acceptance
 303 are required. Nevertheless, a detailed GEANT-based [25] MC simulation was developed
 304 as a tool for the studies of possible systematic effects; this includes full detector geometry
 305 and material description, stray magnetic fields simulation, local DCH inefficiencies, DCH

306 misalignment, and the beam lines simulation (which allows for a reproduction of kaon
 307 momentum spectra and beam profiles). Moreover, time variations of the above effects
 308 during the running period were simulated.

309 A large-scale MC production was carried out for both $K^\pm \rightarrow 3\pi$ decay modes, pro-
 310 viding samples of sizes comparable to those of the data. Namely, $\sim 10^{10}$ events were
 311 generated for each decay mode with the correct balance for each beam and detector con-
 312 figuration closely matching that of the data.

313 **3 Slope difference in $K^\pm \rightarrow 3\pi^\pm$ decay**

314 **3.1 Event reconstruction and selection**

315 Reconstruction of $K^\pm \rightarrow 3\pi^\pm$ events is based on the magnetic spectrometer informa-
 316 tion. Tracks are reconstructed from hits in DCHs using the measured magnetic field
 317 map rescaled to the recorded value of the electric current in the spectrometer analyz-
 318 ing magnet. Systematic uncertainties arising from this procedure due to spectrometer
 319 misalignment and imperfect knowledge of magnetic fields are discussed in Sections 3.2
 320 and 3.3, respectively.

321 Three-track vertices, compatible with the $K^\pm \rightarrow 3\pi^\pm$ decay, are reconstructed using
 322 the Kalman filter algorithm [26] by extrapolation of track segments from the upstream
 323 part of the spectrometer into the decay volume, taking into account multiple scattering in
 324 the Kevlar window and helium volume, and the stray magnetic field in the decay volume
 325 due to the Earth's field and parasitic magnetization of the vacuum tank.

326 The stray field is non-uniform, and has a typical magnitude of 0.5 G (comparable
 327 to the Earth field); the field map was measured in the entire vacuum tank before the
 328 2003 run. Its effect is to induce a transverse deviation of about 1 mm and an angular
 329 deviation of about 10^{-5} rad to a 20 GeV/ c charged particle traversing longitudinally the
 330 whole decay volume. Accounting for the stray field in the vertex reconstruction reduces
 331 the amplitude of the measured sinusoidal variation of the reconstructed $3\pi^\pm$ invariant
 332 mass with respect to the azimuthal orientation of the odd pion by more than an order of
 333 magnitude, to a level below 0.05 MeV/ c^2 . The event kinematics is calculated using the
 334 reconstructed track momenta and directions as extrapolated to the decay vertex.

335 Several stages of compaction and filtering of the data were applied, reducing the data
 336 volume from 200 TB to 1.23 TB, while reducing the number of events in the sample from
 337 18×10^9 to 4.87×10^9 . The applied filtering algorithm includes rejection of low quality
 338 data and also soft kinematic constraints: the main requirement is the presence of at least
 339 3 reconstructed tracks in the event, which rejects about 55% of the recorded triggers.

340 The principal selection criteria applied to the reconstructed variables are listed below.
 341 Note that corrections to track momenta for spectrometer misalignment and magnetic field,
 342 discussed in the following Sections 3.2 and 3.3, are applied before the kinematics of the
 343 event is reconstructed and the selection is made.

- 344 • Total charge of the three pion candidates: $Q = \pm 1$.
- 345 • Total transverse momentum with respect to the z axis: $P_T < 0.3$ GeV/ c , consistent
 346 with the angular spread of the beams and spectrometer resolution.

- 347 • Longitudinal vertex position Z_{vtx} is within the decay volume: $Z_{vtx} > Z_{fc}$, where Z_{fc}
348 is the longitudinal coordinate of the final collimator of the beamline. This condition
349 is imposed since the stray magnetic fields upstream of the final collimator have not
350 been measured, and therefore appropriate corrections can not be made. An upper
351 cut on Z_{vtx} is not imposed, as the geometric acceptance diminishes to zero towards
352 the spectrometer by itself due to the presence of the beam pipe.
- 353 • Transverse decay vertex position within the beam spot: its distance from the z axis
354 $R_{vtx} < 3$ cm.
- 355 • Consistent track timing from DCHs: $|t_i - t_{avg}| < 10$ ns for each track $i = 1, 2, 3$,
356 where $t_{avg} = (t_1 + t_2 + t_3)/3$, which leads to a reasonably low event pile-up probability.
- 357 • Reconstructed kaon momentum is required to be consistent with the beam momen-
358 tum spectrum: $54 \text{ GeV}/c < |\vec{P}_K| < 66 \text{ GeV}/c$.
- 359 • Reconstructed 3π invariant mass: $|M_{3\pi} - M_K| < 9 \text{ MeV}/c^2$, where M_K is the PDG
360 charged kaon mass [7].

361 The distribution of the $3\pi^\pm$ invariant mass (before the cut on that quantity) and its
362 comparison to MC are presented in Fig. 2. The non-Gaussian tails of the mass distribu-
363 tion are mainly due to $\pi^\pm \rightarrow \mu^\pm \nu_\mu$ decay in flight (the spectrometer reconstructing the
364 resulting muon)², which is charge-symmetric. The tails are well understood in terms of
365 MC simulation, and are considered as part of the signal. A deficit of MC events observed
366 in the low mass region does not influence the analysis, since it is mostly outside the signal
367 region; moreover the analysis does not rely on the MC for acceptance computation. Due
368 to the absence of background and the presence of a non-Gaussian contribution of pion
369 decay the selection condition for $M_{3\pi}$ corresponds to five times the resolution.

370 This principal stage of selection leaves a sample of 3.82×10^9 $K^\pm \rightarrow 3\pi^\pm$ events which
371 is practically background free, as $K^\pm \rightarrow 3\pi^\pm$ is the dominant decay mode of the charged
372 kaon with more than one charged particle in the final state. The fact that backgrounds due
373 to other decays of beam kaons and pions are negligible was confirmed by a MC simulation.

374 3.2 Correction for spectrometer misalignment

375 The transverse positions of DCHs and individual wires were measured and realigned at the
376 level of reconstruction software every 2–4 weeks of data taking using data collected during
377 special alignment runs in which muon tracks were recorded with no magnetic field in the
378 spectrometer. This allows an alignment precision of $\sim 30 \mu\text{m}$ to be reached. Spectrometer
379 misalignment itself can not bias the asymmetry measurement. However, time variations
380 of DCH alignment on a short time scale potentially can, since an uncorrected shift of a
381 DCH along the x axis leads to charge-antisymmetric mismeasurement of the momenta.

382 An unambiguous measure³ of the residual transverse horizontal misalignment is the
383 difference between the average reconstructed 3π invariant masses corresponding to decays
384 of K^+ and K^- , denoted as $\Delta\bar{M}$. The following sensitivities were determined from the

²The shape and size of the non-Gaussian tails notably depend on the adopted cuts on vertex transverse position and total transverse momentum.

³Assuming CPT conservation.

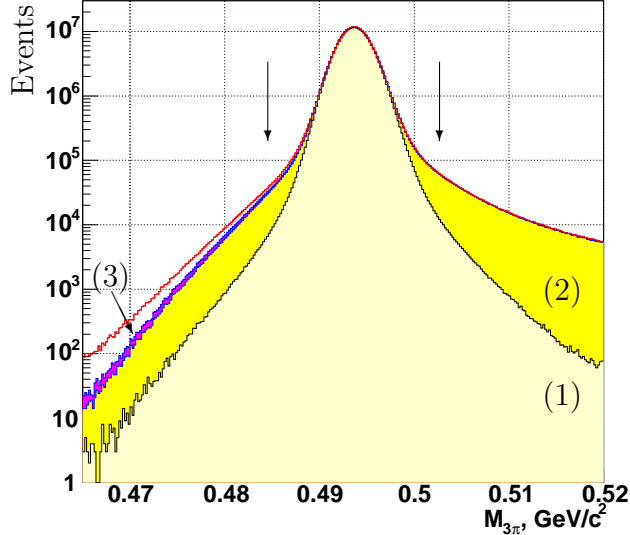


Figure 2: Reconstructed spectrum of $3\pi^\pm$ invariant mass (upper envelope curve) and its comparison to normalized MC components: (1) events without $\pi \rightarrow \mu\nu$ decay in flight, (2) events with $\pi \rightarrow \mu\nu$ decay, (3) radiative $K_{3\pi\gamma}$ events. The selection conditions are marked with vertical arrows. The deficit of MC events in the low mass area is mostly outside the signal region.

385 data: a shift of the DCH4 along the x axis by $1 \mu\text{m}$ with respect to its nominal position
 386 induces a measured mass difference of $\Delta\bar{M} = 1.4 \text{ keV}/c^2$; a difference of $1 \mu\text{m}$ between
 387 the DCH4 x -positions between the data sets taken with opposite spectrometer polarities
 388 induces a fake slope difference of $\delta(\Delta g^c) = 0.03 \times 10^{-4}$. Sensitivities to shifts of the other
 389 DCHs are similar.

390 Monitoring of $\Delta\bar{M}$ revealed significant transverse movements of the DCHs between the
 391 individual alignment runs, at a rate of typically below $\sim 5\mu\text{m}/\text{day}$ and never exceeding
 392 $20 \mu\text{m}/\text{day}$ ⁴, which introduces spurious slope differences of the order of a few units of
 393 10^{-5} . Introduction of time-dependent corrections to the measured momenta based on the
 394 observed $\Delta\bar{M}$ reduces these fake slope differences by more than an order of magnitude to
 395 a negligible level of $\delta(\Delta g^c) < 0.1 \times 10^{-4}$.

396 3.3 Effects due to spectrometer magnetic field

397 The measurement of pion momenta is based on the knowledge of the magnetic field in
 398 the spectrometer magnet. The variation of the current in the magnet biases the overall
 399 momentum scale of the spectrometer. This variation can be directly measured with
 400 a relative precision of 5×10^{-4} ; smaller variations are continuously monitored with a
 401 precision of $\sim 10^{-5}$ using the deviation of the reconstructed charge-averaged kaon mass
 402 from the nominal PDG value [7]. A time-dependent correction can be introduced by
 403 scaling the reconstructed track momenta symmetrically for positive and negative tracks.
 404 However, the momentum scale effects are a priori highly charge-symmetric by design, due
 405 to the simultaneous K^+ and K^- beams (this was also explicitly verified by comparing the

⁴On an exceptional occasion during the 2003 data taking, a DCH position shifted by $200\mu\text{m}$ in one day.

406 results obtained with and without the correction). Therefore no correction was applied
 407 for spectrometer current.

408 On the contrary, the effects caused by a non-uniform permanent (not inverting with the
 409 spectrometer magnetic field polarity) component of the magnetic field in the region of the
 410 spectrometer magnet are potentially charge asymmetric. They were studied by artificially
 411 introducing the corresponding distortions to measured track momenta depending on the
 412 coordinates of impact points in the magnetic plane, consistent with the measurement
 413 precision of the magnetic field map and the expected size of the permanent field (~ 1 G).
 414 The resulting variation of the result of $\delta(\Delta g^e) = 0.3 \times 10^{-4}$ was considered as a residual
 415 systematic uncertainty due to this effect.

416 Remarkably, a statistically significant Δg^e measured with the events from the side
 417 bands of $3\pi^\pm$ mass distribution (i.e. outside the signal region) can be achieved by intro-
 418 ducing certain realistic configurations of a non-uniform permanent magnetic field in the
 419 region of the spectrometer magnet.

420 3.4 Correction for instability of beam geometry

421 The geometric acceptance for the $K^\pm \rightarrow \pi^\pm \pi^+ \pi^-$ decays is mainly determined by the
 422 vacuum beam pipe traversing the centres of the DCHs, and the material in the central
 423 region of each DCH where certain groups of DCH wires terminate⁵. Moreover, the beam
 424 optics can only control the average transverse beam positions to ± 1 mm. Time variations
 425 of the transverse beam positions within the mentioned precision generate a sizable charge-
 426 asymmetric bias to the acceptance inducing instrumental slope asymmetries of the order
 427 of a few units of 10^{-4} . It would require a stability of the transverse beam positions to the
 428 level of $100 \mu\text{m}$ in order to reduce the bias to a negligible level. However it is possible to
 429 determine the average K^+ and K^- beam positions as functions of time to this order of
 430 precision and apply charge symmetric cuts, as explained below.

431 Inner DCH geometrical acceptance cuts which fully contain the beam pipe and the
 432 surrounding DCH regions are applied to the positions of pion impact points $\vec{R}_{\pi i}^{1,4}$ in the
 433 planes of DCH1 and DCH4 relative to the average beam intercepts in the DCH planes.
 434 These vary slightly with time and differ for K^+ and K^- .

435 The transverse coordinates of a beam kaon $\vec{R}_0^{1,2}$ in the planes of DCH1 and DCH2
 436 for each event are reconstructed as the momentum-weighted averages of the coordinates
 437 $\vec{R}_{\pi i}^{1,2}$ of the three reconstructed pions: $\vec{R}_0^{1,2} = \sum_{i=1}^3 (\vec{R}_{\pi i}^{1,2} |\vec{P}_{\pi i}|) / \sum_{i=1}^3 |\vec{P}_{\pi i}|$, where $|\vec{P}_{\pi i}|$ is
 438 reconstructed momentum of a pion. Transverse coordinates of a beam kaon in the plane of
 439 DCH4 \vec{R}_0^4 corresponding to absence of the bending by the analyzing magnet are computed
 440 by linear extrapolation using \vec{R}_0^1 and \vec{R}_0^2 .

441 The average beam positions in the planes of DCH1 and DCH4 $\langle \vec{R}_0^{1,4} \rangle$ are computed on
 442 the basis of the distributions of \vec{R}_0^1 and \vec{R}_0^4 for the selected event sample. A bias introduced
 443 to $\langle \vec{R}_0^{1,4} \rangle$ by the fact that $|\vec{R}_{\pi i}^{1,2}|$ and $|\vec{P}_{\pi i}|$ are themselves affected by the acceptance is
 444 negligible. A database of the average beam positions $\langle \vec{R}_0^{1,4} \rangle$ depending on kaon sign, time
 445 (excursions of ~ 1 mm), kaon momentum (excursions of ~ 1 mm in the horizontal plane,
 446 ~ 1 cm in the vertical plane), and time within SPS spill (excursions of ~ 1 mm) was
 447 created.

⁵Due to a relatively small Q -value of the $K^\pm \rightarrow 3\pi^\pm$ decay, $Q = 75.0$ MeV, the outer edges of the DCHs do not bias the acceptance.

448 The conditions $|\vec{R}_{\pi i}^{1,4} - \langle \vec{R}_0^{1,4} \rangle| > 11.5$ cm, $i = 1, 2, 3$, are applied to symmetrize the
 449 beam geometry effects. These cuts cost 12% of the statistics, leading to a sample of
 450 3.36×10^9 events. The minimum distance of 11.5 cm is chosen to ensure that the region
 451 of the beam pipe and the adjacent central insensitive areas of the DCHs are securely
 452 excluded by the cut.

453 The residual systematic effects arise from the stray magnetic field in the decay volume,
 454 which deflects $\vec{R}_{\pi i}^{1,4}$ with respect to $\langle \vec{R}_0^{1,4} \rangle$ in a charge-antisymmetric way. Corrections for
 455 the stray field to the measured $\vec{R}_0^{1,4}$ were performed. However, the precision of these
 456 corrections is limited by the precision of magnetic field measurement, which leads to a
 457 residual systematic uncertainty of $\delta(\Delta g^c) = 0.2 \times 10^{-4}$.

458 3.5 Correction for trigger inefficiency

459 Only charge-asymmetric trigger inefficiencies correlated with u can possibly bias the mea-
 460 surement. Inefficiencies of the individual trigger components were directly measured as
 461 functions of u using control data samples from prescaled low bias triggers collected along
 462 with the main ones. This allowed for an accounting for time variations of the efficiencies,
 463 and for a propagation of the statistical errors of the measured inefficiencies into the final
 464 result.

465 The trigger logic is described in Section 1.3. The control trigger condition for the L1
 466 efficiency measurement requires at least one coincidence of hits in the two planes of the
 467 HOD. The control triggers for the L2 efficiency measurement are L1 triggers recorded
 468 regardless of the L2 response. The statistics of each of the two control samples is roughly
 469 1% of the main sample⁶.

470 The L1 trigger condition requires the coincidence of hits in two of the 16 non-overlapping
 471 HOD segments. This condition is loose as there are three charged particles in a fully re-
 472 constructed event, and the resulting inefficiency is low. It was measured to be 0.9×10^{-3}
 473 and found to be stable in time. Due to a few short-term malfunctions of a HOD channel,
 474 several subsamples of the data sample are affected by higher inefficiency (up to 7×10^{-3}),
 475 the source of the inefficiency being localized in space. This kind of inefficiency was re-
 476 duced (and symmetrized) in the selected data sample by applying appropriate geometric
 477 cuts to the pion impact points on the hodoscope surface for the relevant supersamples.
 478 This procedure led to the loss of 7.1% of the statistics, reducing the final sample to
 479 3.11×10^9 events. Due to good time stability of the L1 inefficiency, no bias from the L1
 480 trigger is assumed. An overall uncertainty of the L1 bias was conservatively estimated to
 481 $\delta(\Delta g^c) = 0.3 \times 10^{-4}$, limited by the statistics of the control sample.

482 Two components of the L2 trigger inefficiency were identified: one due to trigger timing
 483 misalignment, and the other due to local DCH inefficiency (so called “geometrical”). The
 484 part related to timing misalignment has a size of $\sim 0.2\%$, and a priori does not affect the
 485 result, being uncorrelated to the kinematic variables. Its charge symmetry was checked
 486 with a detailed MC simulation of pile-up effects, and a study of the dependence of the
 487 result on the number of allowed accidental tracks. On the contrary, the geometrical part
 488 is correlated to event kinematics, and varies in time due to variations of the local DCH
 489 inefficiencies. These inefficiencies affect the trigger more than the offline reconstruction

⁶Sizes of the control samples are adequate to measure trigger inefficiencies with a precision better than the statistical error, due to sufficiently low trigger inefficiencies.

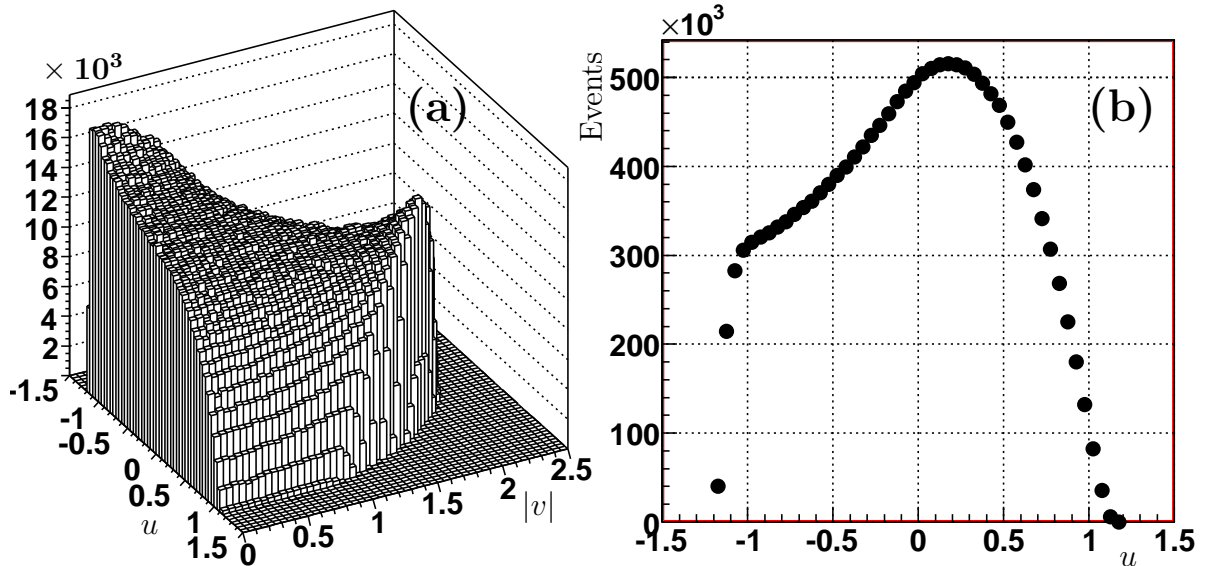


Figure 3: (a) Reconstructed distribution of the selected $K^\pm \rightarrow \pi^\pm \pi^+ \pi^-$ events in the kinematic variables $(u, |v|)$; (b) its projection to the u axis. The distributions correspond to a fraction of the data sample.

490 due to lower redundancy and worse online resolutions. For this reason the measured u
 491 spectra are corrected for this part of the inefficiency. The size of the inefficiency for the
 492 selected sample was measured to be close to 0.6×10^{-3} , but some periods are affected by
 493 higher inefficiency of up to 1.5% (its sources not being localized in space in a simple way).
 494 The correction to the whole statistics amounts to $\Delta(\Delta g^c) = (-0.1 \pm 0.3) \times 10^{-4}$, where
 495 the error is statistical owing to the limited size of the control sample.

496 The above procedure leads to over-estimation of the systematic uncertainties related
 497 to trigger inefficiencies, since the correlations of trigger inefficiencies in bins of u (in other
 498 words, smoothness of variation of trigger efficiency over u) are not taken into account.

499 3.6 Fits to Δg^c and cross checks

500 The reconstructed Dalitz plot distribution of the events passing the selection and the
 501 corrections described in the previous Sections (corresponding to a fraction of the sample)
 502 is presented in Fig. 3a. Its projection to the u axis is presented in Fig. 3b⁷.

503 The quadruple ratios of the u spectra (5) were computed, and Δg^c was measured by
 504 the two methods described in Section 2.5 by fitting with the function (6). The values of
 505 slope parameters $g^c = -0.21134$, $h^c = 0.01848$ recently measured by NA48/2 [24] using
 506 55% of the 2003 data sample, and consistent with the world averages, were used. The
 507 uncertainties on the values of the above slope parameters lead to negligible effects on the
 508 result.

509 The grand quadruple ratio obtained by averaging quadruple ratios over supersamples
 510 in each bin of u (corrected for L2 trigger efficiency) is tabulated in Table 1, and presented

⁷The eight u spectra corresponding to various combinations of kaon sign and magnetic field polarities involved into the computation are not presented separately, since the corresponding systematic biases are small, and the differences between the spectra are difficult to see by eye.

Table 1: The quadruple ratio $R_4^c(u)$ corrected for L2 inefficiency averaged over the super-samples.

u bin centre	Content	Error	u bin centre	Content	Error
-1.45	8.96034	0.52320	-0.05	10.37140	0.00730
-1.35	10.28018	0.12639	0.05	10.38555	0.00729
-1.25	10.39128	0.03900	0.15	10.37973	0.00730
-1.15	10.35639	0.01459	0.25	10.37140	0.00741
-1.05	10.38233	0.00983	0.35	10.37868	0.00755
-0.95	10.38593	0.00883	0.45	10.38286	0.00777
-0.85	10.38105	0.00855	0.55	10.36338	0.00805
-0.75	10.37476	0.00834	0.65	10.38241	0.00849
-0.65	10.38148	0.00815	0.75	10.37654	0.00907
-0.55	10.37467	0.00798	0.85	10.38572	0.00992
-0.45	10.36193	0.00780	0.95	10.40517	0.01137
-0.35	10.37647	0.00764	1.05	10.38179	0.01434
-0.25	10.37972	0.00747	1.15	10.35615	0.02568
-0.15	10.37670	0.00734	1.25	10.18942	0.25256

511 along with the result of the corresponding fit in Fig. 4.

512 The results of the independent fits for each supersample, including the numbers of
513 events selected, the “raw” values of Δg^c obtained without applying the trigger corrections,
514 and the final values of Δg^c with the L2 trigger corrections applied are presented in Table 2.
515 The independent results obtained for the nine supersamples are shown in Fig. 5(a): the
516 individual measurements of Δg^c are statistically compatible with a $\chi^2/\text{ndf} = 9.7/8$.

517 The measured control quantities $\Delta g_{S,J}^c$ and Δg_{UD}^c , which are the slopes of the control
518 ratios (7) and (8), for the nine supersamples are presented in Fig. 5(b) and 5(c), respec-
519 tively (data points are overlaid with MC ones). The sizes of these slopes induced by
520 residual time-variable imperfections of the apparatus which cancel in the result (5) are
521 of the same order of magnitude as the statistical errors (10^{-4}), indicating that second
522 order effects which could induce non-zero values for them are negligible. Moreover, the
523 comparison with MC simulations shows that the sizes of the apparatus asymmetries are
524 well understood in terms of local inefficiencies and variations of beam optics.

525 3.7 Residual systematic effects

526 Effects due to the difference of cross sections of π^+ and π^- hadronic interactions with the
527 material of the detector were evaluated by a simulation of $K \rightarrow 3\pi$ decays taking into
528 account a parameterized energy dependence of cross sections of $\pi^\pm N$ interactions [7, 27]
529 and the material composition of the detector. As the most striking example of the effect
530 of the charge asymmetry of $\pi^\pm N$ cross sections, a $\pi^- p$ interaction in the first plastic
531 scintillator plane of the HOD, giving rise to a fully neutral final state, produces a trigger
532 bias for $K^- \rightarrow \pi^- \pi^0 \pi^0$ decays relative to $K^+ \rightarrow \pi^+ \pi^0 \pi^-$ decays. Owing to the kaon
533 momentum spectrum, π^\pm momentum in the detector is restricted to $p_\pi > 5 \text{ GeV}/c$, which
534 1) validates the use of the cross section parameterization, and 2) makes the measurement

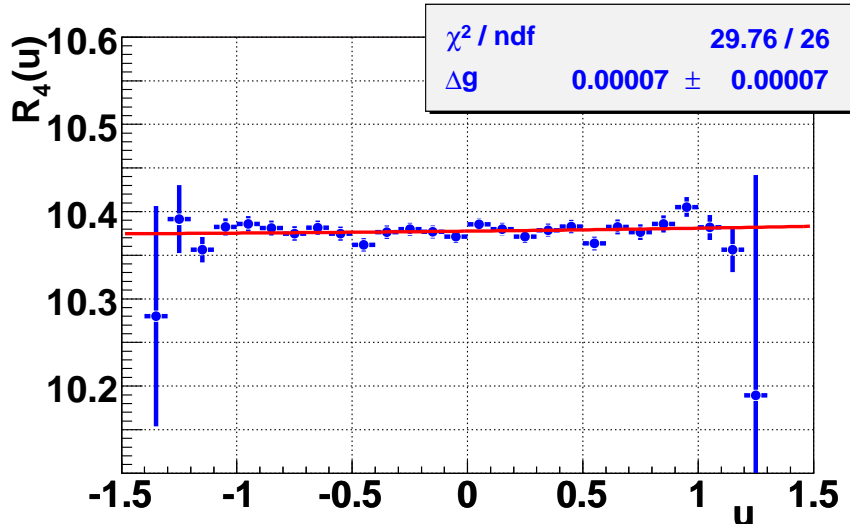


Figure 4: The quadruple ratio $R_4^c(u)$ corrected for L2 trigger efficiency averaged in bins of u over supersamples fitted with the function (6) with $g^c = -0.21134$, $h^c = 0.01848$ [24]. The point in the first bin, given in the Table 1, is out of the vertical range.

535 insensitive to the largest differences between π^+p and π^-p cross sections occurring at
 536 $p_\pi \sim 1 \text{ GeV}/c$. The integral charge-asymmetric effects were found to be of the order of
 537 10^{-4} , however their u -dependence was found to be negligible, inducing a bias of only the
 538 order of $\Delta g \sim 10^{-6}$.

539 The effects due to the difference of K^+ and K^- production spectra by the primary
 540 protons [28] do not cancel in the quadruple ratio. The difference between the K^+ and K^-
 541 spectra was quantified by measuring the slope of the quadruple ratio of the reconstructed
 542 K^+ and K^- momentum spectra. The slope of the K^+/K^- spectra ratio $f(p)$ normalized
 543 by $f(60 \text{ GeV}) = 1$ was determined to be $df(p)/dp = 0.6\%/(\text{GeV}/c)$. This induces charge
 544 asymmetry of geometrical acceptance leading to a fake slope difference of $\delta(\Delta g^c) = 0.3 \times$
 545 10^{-3} , as estimated by a MC simulation. This value was conservatively taken as the
 546 corresponding systematic uncertainty.

547 Taking into account that the composition of the beams is not charge symmetric (in
 548 particular, the K^+ and K^- fluxes differ), event distortions caused by pile-up with the
 549 products of another kaon decay or a beam halo particle traversing the sensitive region
 550 of the spectrometer is a potential source of systematic bias. To study the pile-up effects
 551 an accidental activity generator was introduced into the MC. This generator was tuned
 552 using the measured composition of beam and halo fluxes, and a production of $\sim 10^8$
 553 correlated pairs of an original kaon decay event and a piled-up event was carried out. No
 554 charge-asymmetric effects were observed in the reconstructed u distributions nor in the
 555 L2 trigger inefficiencies down to a level of $\delta(\Delta g^c) = 0.2 \times 10^{-4}$, limited by MC statistics.

556 Biases due to resolution effects were studied by using various methods of expressing
 557 the u variable in terms of directly measured quantities (using only the invariant mass of
 558 the pair of even pions in the laboratory frame; using the energy of the odd pion in the
 559 kaon rest frame; using a 3C kinematic fit constraining kaon mass and direction) differing
 560 in resolution as a function of u . Stability of the result with respect to variation of bin
 561 size in u has been studied as well. An estimate for the systematic uncertainty due to
 562 resolution effects of $\delta(\Delta g^c) = 0.2 \times 10^{-4}$ has been obtained.

Table 2: Statistics selected in each supersample and measured Δg^c : “raw” and corrected for L2 trigger inefficiency. The errors are statistical only; the errors in the last column include the L2 trigger efficiency errors.

Supersample	$K^+ \rightarrow \pi^+\pi^+\pi^-$ decays in 10^6	$K^- \rightarrow \pi^-\pi^-\pi^+$ decays in 10^6	$\Delta g^c \times 10^4$ raw	$\Delta g^c \times 10^4$ corrected
0	448.0	249.7	0.7 ± 1.4	-0.4 ± 1.8
1	270.8	150.7	-0.8 ± 1.8	-0.8 ± 1.8
2	265.5	147.8	-1.4 ± 2.0	-1.3 ± 2.0
3	86.1	48.0	0.6 ± 3.2	1.3 ± 3.3
4	232.5	129.6	-2.7 ± 1.9	-1.6 ± 2.2
5	142.4	79.4	5.0 ± 2.5	4.8 ± 2.6
6	193.8	108.0	4.9 ± 2.1	4.9 ± 2.2
7	195.9	109.1	1.4 ± 2.1	1.3 ± 2.1
8	163.9	91.4	1.4 ± 2.3	0.5 ± 2.3
Total	1998.9	1113.7	0.8 ± 0.7	0.7 ± 0.7

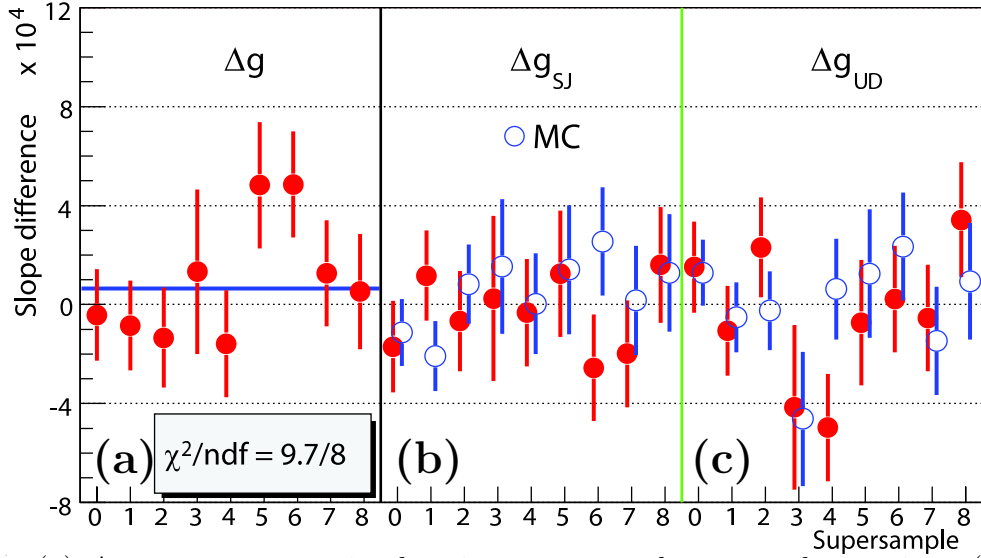


Figure 5: (a) Δg^c measurement in the nine supersamples; control quantities (b) Δg_{SJ}^c and (c) Δg_{UD}^c corresponding to detector and beam line asymmetries which cancel in the quadruple ratio, and their comparison to MC (open circles).

Table 3: Systematic uncertainties and the correction for L2 trigger inefficiency for Δg^c measurement.

Systematic effect	Correction, uncertainty $\delta(\Delta g^c) \times 10^4$
Spectrometer misalignment	± 0.1
Spectrometer magnetic field	± 0.3
Beam geometry and stray magnetic fields	± 0.2
Kaon production spectra	± 0.3
Pile-up	± 0.2
Resolution and fitting	± 0.2
Total purely systematic uncertainty	± 0.6
L1 trigger inefficiency	± 0.3
L2 trigger inefficiency	-0.1 ± 0.3

3.8 The resulting A_g^c

563

564 A summary of the systematic uncertainties, including a correction for L2 trigger inef-
565 ficiency, is presented in Table 3. The difference in the linear slope parameter of the
566 Dalitz plot of the $K^\pm \rightarrow \pi^\pm \pi^+ \pi^-$ decays, measured with the full NA48/2 data sample of
567 3.11×10^9 events, is found to be

$$\Delta g^c = g^+ - g^- = (0.7 \pm 0.7_{stat.} \pm 0.4_{trig.} \pm 0.6_{syst.}) \times 10^{-4}. \quad (9)$$

568 Here the individual systematic errors are added in quadrature, and the errors due to
569 trigger inefficiencies are of statistical nature. Converted to the direct CP violating charge
570 asymmetry (3) using the value of the Dalitz plot slope $g^c = -0.21134 \pm 0.00017$ recently
571 measured by the NA48/2 [24],

$$A_g^c = (-1.5 \pm 1.5_{stat.} \pm 0.9_{trig.} \pm 1.3_{syst.}) \times 10^{-4} = (-1.5 \pm 2.2) \times 10^{-4}. \quad (10)$$

4 Slope difference in $K^\pm \rightarrow \pi^\pm \pi^0 \pi^0$ decay

572

4.1 Event reconstruction and selection

573

574 The $K^\pm \rightarrow \pi^\pm \pi^0 \pi^0$ decays are reconstructed considering $\pi^0 \rightarrow \gamma\gamma$ decays of each of the
575 π^0 s and hence the reconstruction of the four photons is required. The principal selection
576 criteria are described below.

- 577 • An energy deposition cluster in the LKr is considered to correspond to a photon
578 candidate if the following conditions are fulfilled: 1) it has an energy $E > 3$ GeV,
579 which minimizes effects of nonlinearity of the LKr response (typically 2% at 3 GeV
580 and becoming negligible above 10 GeV); 2) it is situated at distances larger than 10
581 cm from other clusters, and at distances larger than 15 cm from impact points of the
582 reconstructed charged particles, which minimizes effects of energy sharing between
583 the reconstructed clusters due to overlap; 3) it satisfies requirements on distances
584 from the outer LKr edges and the beam pipe, which ensures full lateral containment
585 of the electromagnetic showers.

- 586 • The event is required to have at least one reconstructed track of a charged particle,
587 and at least four photon candidates.
- 588 • To suppress the charge-asymmetric DCH acceptance bias induced by the time in-
589 stability of beam geometry, cuts are applied to distances between the track impact
590 points in DCH1 and DCH4 planes $\vec{R}_\pi^{1,4}$ and the average reconstructed beam posi-
591 tions $\langle \vec{R}_0^{1,4} \rangle$. These cuts are similar to those applied in the $K^\pm \rightarrow \pi^\pm \pi^+ \pi^-$ analysis;
592 the rationale and a description are contained in Section 3.4.

593 For each selected event, a $K^\pm \rightarrow \pi^\pm \pi^0 \pi^0$ decay is reconstructed as follows. Assuming
594 that a pair of photon candidates i, j ($i, j = 1, 2, 3, 4$) originates from a $\pi^0 \rightarrow \gamma\gamma$ decay
595 occurring at a distance D_{ij} from the LKr front face, then D_{ij} is calculated to very good
596 approximation as $D_{ij} = R_{ij} \sqrt{E_i E_j} / m_{\pi^0}$, where E_i and E_j are the energies of the i -th and
597 j -th photon candidates, R_{ij} is the distance between their impact points at the LKr front
598 plane, and m_{π^0} is the PDG π^0 mass [7].

599 To search for two $\pi^0 \rightarrow \gamma\gamma$ decays occurring at the same point of the decay volume,
600 among all the combinations of non-overlapping photon candidate pairs (i, j) and (k, l) the
601 one with the smallest value of $|D_{ij} - D_{kl}|$ is selected. Moreover, the smallest of $|D_{ij} - D_{kl}|$
602 is required to be less than 500 cm, while the resolution on the difference $D_{ij} - D_{kl}$ for
603 photon pairs originating from the same point of space is ~ 100 cm. For the best selected
604 (if any) combination (i, j) and (k, l) , the value of $(D_{ij} + D_{kl})/2$ is used to define the
605 longitudinal position of a K^\pm decay vertex Z_{vtx} .

606 No geometrical information about the π^\pm track is used for vertex reconstruction in
607 order to avoid the related charge-asymmetric biases induced by beam geometry variation
608 and stray magnetic fields.

609 The following selection criteria are applied to the reconstructed event kinematics.

- 610 • The longitudinal vertex position required to be within the decay volume: $Z_{vtx} > Z_{fc}$,
611 where Z_{fc} is the longitudinal coordinate of the final collimator.
- 612 • Consistent photon and track timing: $|t_{avg}^\gamma - t_i^\gamma| < 5$, $|t_{avg}^\gamma - t^\pm| < 20$ ns, where t_i^γ
613 are times of the four selected LKr clusters, t^\pm is the time of the selected track, and
614 $t_{avg}^\gamma = \sum t_i^\gamma / 4$.
- 615 • Reconstructed kaon momentum is required to be consistent with the beam momen-
616 tum spectrum: $54 \text{ GeV}/c < |\vec{P}_K| < 66 \text{ GeV}/c$.
- 617 • Reconstructed 3π invariant mass: $|M_{3\pi} - M_K| < 6 \text{ MeV}/c^2$. This cut is narrower
618 than in the $K^\pm \rightarrow 3\pi^\pm$ case due to a better mass resolution.

619 The above requirements lead to the final sample of 9.13×10^7 events. Fig. 6 shows
620 the $\pi^\pm \pi^0 \pi^0$ invariant mass distribution (before a cut on this quantity). The resolution on
621 the invariant mass is $0.9 \text{ MeV}/c^2$. The tails of the mass distribution originate from wrong
622 photon pairing (the fraction of these events estimated by a MC simulation is 0.2%) and
623 $\pi \rightarrow \mu\nu$ decays. The background is negligible for the applied mass cut.

624 It can be seen from (2) that the kinematic variable u can be computed using only the
625 $\pi^0 \pi^0$ invariant mass. Thus a measurement of u uses the information from the LKr only,
626 not involving the DCH data. This provides a certain charge symmetry of the procedure,

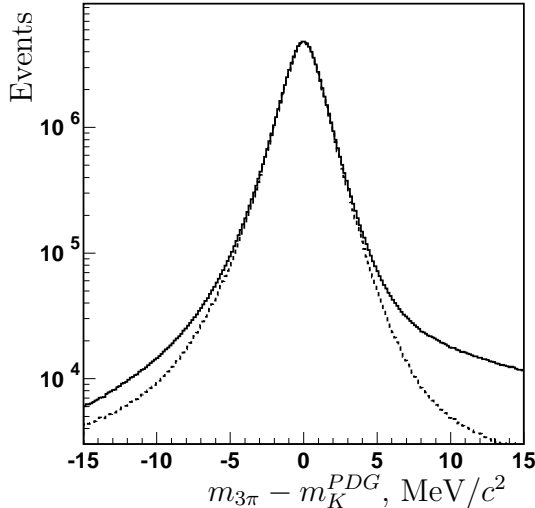


Figure 6: Deviation of the reconstructed $\pi^\pm\pi^0\pi^0$ invariant mass from the PDG kaon mass [7]. The dashed histogram shows the same distribution for events with no hits in the muon detector (not used in the analysis).

627 as the LKr is a “charge blind” subdetector, except for effects of small differences between
 628 π^+ and π^- interaction characteristics.

629 The reconstructed Dalitz plot distribution of the selected events is shown in Fig. 7(a),
 630 and its projection on the u axis is presented in Fig. 7(b).

631 4.2 Fits to Δg^n and cross checks

632 Quadruple ratios of the u spectra (5) were computed, and Δg^n was measured by the two
 633 methods described in Section 2.5 involving fitting with the function (6). The nominal val-
 634 ues of slope parameters $g^n = 0.626$, $h^n = 0.052$ [7] were used. Unlike the $K^\pm \rightarrow \pi^\pm\pi^+\pi^-$
 635 case, no trigger corrections to the u spectra are required, as discussed in Section 4.4.

636 A grand quadruple ratio obtained by averaging quadruple ratios over supersamples
 637 in every bin of u is tabulated in Table 4, and presented along with the result of the
 638 corresponding fit in Fig. 8.

639 Numbers of selected events and the results of the fits in every supersample are pre-
 640 sented in Table 5. The independent results obtained in the seven supersamples are shown
 641 in Fig. 9(a): the individual measurements are compatible with a $\chi^2/\text{ndf} = 1.5/6$.

642 The measured control quantities $\Delta g_{S^J}^n$ and Δg_{UD}^n , which are the slopes of the control
 643 ratios (7) and (8), in the seven supersamples are presented in Fig. 9(b) and (c), respectively
 644 (data points are overlaid with MC ones). These instrumental asymmetries do not exceed
 645 the size of the statistical errors, and are well reproduced by the MC simulation.

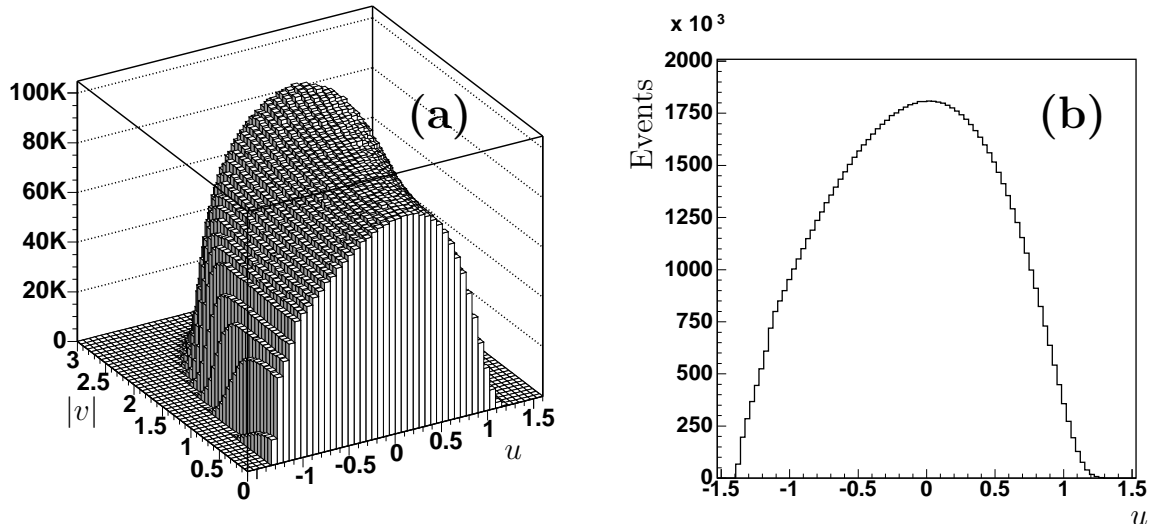


Figure 7: (a) Reconstructed Dalitz plot distribution in the kinematic variables $(u, |v|)$ for the selected $K^\pm \rightarrow \pi^\pm \pi^0 \pi^0$ events; (b) u -spectrum for the selected events.

4.3 Systematic effects due to calorimeter performance

646

647 As discussed above, the LKr calorimeter is the primary detector for $K^\pm \rightarrow \pi^\pm \pi^0 \pi^0$ decay
 648 reconstruction, and the only detector used for measurement of the variable u . The only
 649 charge-asymmetric effect in LKr performance is related to the difference between π^+ and
 650 π^- interaction cross sections. Variation of the cut on the minimum allowed distance
 651 between the photon candidate clusters and the impact point of the charged track on LKr
 652 front face led to a conservative estimation of the corresponding systematic uncertainty:
 653 $\delta(\Delta g^n) = 0.5 \times 10^{-4}$. Introduction of a shower energy sharing correction leads to a
 654 consistent estimate.

655

Other effects related to the LKr reconstruction are not expected to induce fake charge
 656 asymmetries. However the following stability checks were performed.

657

- Stability with respect to variation of the resolution on the reconstructed u variable for K^+ and K^- decays was studied with a large sample of events simulated by MC. The result was found to be stable within 0.1×10^{-4} .

658

659

660

- The result is stable to 0.1×10^{-4} with respect to introducing various ways of correcting the measured photon energies to account for nonlinearity of the LKr response at low energy.

661

662

663

- The effect of wrong photon pairing in the reconstruction of the $\pi^0 \pi^0$ pair was studied by a large sample of simulated events. The result was found stable to better than 0.1×10^{-4} .

664

665

666

- The result was found to have negligible sensitivity to variation of the cluster radial distance cut value around the beam pipe.

667

Table 4: The quadruple ratio $R_4^n(u)$ averaged over supersamples.

u bin centre	Content	Error	u bin centre	Content	Error
-1.35	10.2110	0.1248	0.05	10.4213	0.0381
-1.25	10.2762	0.0775	0.15	10.3864	0.0382
-1.15	10.4234	0.0621	0.25	10.4363	0.0389
-1.05	10.5216	0.0552	0.35	10.3485	0.0393
-0.95	10.4020	0.0504	0.45	10.4804	0.0411
-0.85	10.4261	0.0474	0.55	10.4494	0.0430
-0.75	10.3868	0.0449	0.65	10.4222	0.0458
-0.65	10.4322	0.0432	0.75	10.4725	0.0507
-0.55	10.3885	0.0415	0.85	10.4576	0.0584
-0.45	10.3781	0.0403	0.95	10.4599	0.0726
-0.35	10.4039	0.0395	1.05	10.3386	0.1028
-0.25	10.3408	0.0386	1.15	10.1208	0.1912
-0.15	10.4057	0.0383	1.25	10.1472	0.5851
-0.05	10.4262	0.0382	1.35	8.8335	2.7018

4.4 Uncertainties due to trigger inefficiency

The trigger logic is described in Section 1.3. Charge symmetry of every trigger component was studied either by direct measurement using samples recorded with low bias control triggers, or by simulation, as discussed below.

The inefficiency of the HOD component of the L1N trigger, which is due to inefficiency of the HOD counters, was measured using a control sample of all events with exactly one reconstructed track, triggered by conditions requiring activity in the LKr. The integral inefficiency for the selected $K^\pm \rightarrow \pi^\pm \pi^0 \pi^0$ sample was measured to be about 0.25%. It increased up to 2.0% during short periods due to malfunctioning of a few HOD counters; this effect was reduced and symmetrized, as described in Section 3.5. The measured map of inefficiency measured as a function of the (x, y) coordinates at the HOD plane allowed

Table 5: Selected statistics and measured Δg^n in each supersample.

Supersample	$K^+ \rightarrow \pi^+ \pi^0 \pi^0$ decays in 10^6	$K^- \rightarrow \pi^- \pi^0 \pi^0$ decays in 10^6	$\Delta g^n \times 10^4$
I	16.40	9.14	3.4 ± 3.9
II	10.17	5.66	0.6 ± 5.1
III	3.71	2.06	-3.0 ± 8.4
IV	5.15	2.87	4.8 ± 7.1
V	8.88	4.94	4.1 ± 5.3
VI	7.49	4.17	4.1 ± 5.8
VII	6.86	3.82	-2.1 ± 6.0
Total	58.66	32.66	2.2 ± 2.1

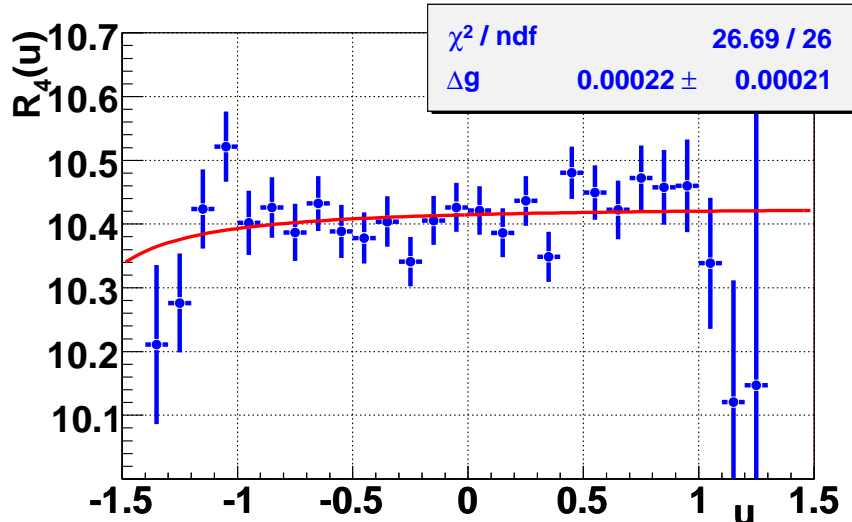


Figure 8: The quadruple ratio $R_4^n(u)$ averaged by supersamples in bins of u fitted with the function (6) with $g^n = 0.626$, $h^n = 0.052$ [7].

679 a precise estimation of trigger inefficiency effect to be made. It was found to be consistent
 680 with no spurious asymmetry at the level of $\delta(\Delta g^n) = 0.1 \times 10^{-4}$.

681 The inefficiency of the LKr component of the L1N trigger was measured with a sample
 682 of minimum bias triggers. It amounted to 0.7% in supersamples I and II, and 3% in
 683 supersamples III and IV. For supersamples V, VI and VII the L1N condition was relaxed
 684 to compensate for the above degradation by adding in “OR” a condition requiring the total
 685 LKr energy deposition to exceed 15 GeV to the initial condition based on the presence
 686 of at least two clusters, which resulted in a stable inefficiency of 0.03%. The degradation
 687 of the trigger performance at the beginning of supersample III was later identified to be
 688 due to a small time misalignment between parts of the hardware trigger logic.

689 The inefficiency of the LKr component of L1N is a priori charge symmetric, since it is
 690 based on LKr energy deposit conditions. To confirm this, the inefficiency has been studied
 691 using a MC simulation, with an LKr map of local trigger inefficiency (measured directly
 692 from the data) used as a reference. Several checks have been performed, in particular by
 693 artificially increasing the measured inefficiency or by including totally inefficient regions.
 694 No systematic effects have been observed at a level of $\delta(\Delta g^n) = 0.1 \times 10^{-4}$, which is
 695 considered a systematic uncertainty due to the LKr component of the L1 trigger.

696 The inefficiency of the L2N trigger was mostly due to local inefficiencies of the DCHs,
 697 and varied from 4% to 6%. The effects due to such inefficiencies, being of geometrical
 698 nature, have been simulated by a MC. No charge asymmetry was found; upper limits of
 699 systematic uncertainties from other (smaller) possible effects, including those related to
 700 variations of timing offsets between subdetectors and data buffer overflows, were estimated
 701 directly by variation of the selection conditions. The total systematic uncertainty induced
 702 by L2N inefficiency was estimated not to exceed $\delta(\Delta g^n) = 0.3 \times 10^{-4}$.

703 4.5 Other systematic effects

704 Effects related to the magnetic spectrometer do not affect the result significantly, since
 705 the charged track is only used for the identification of the kaon charge and in the mass

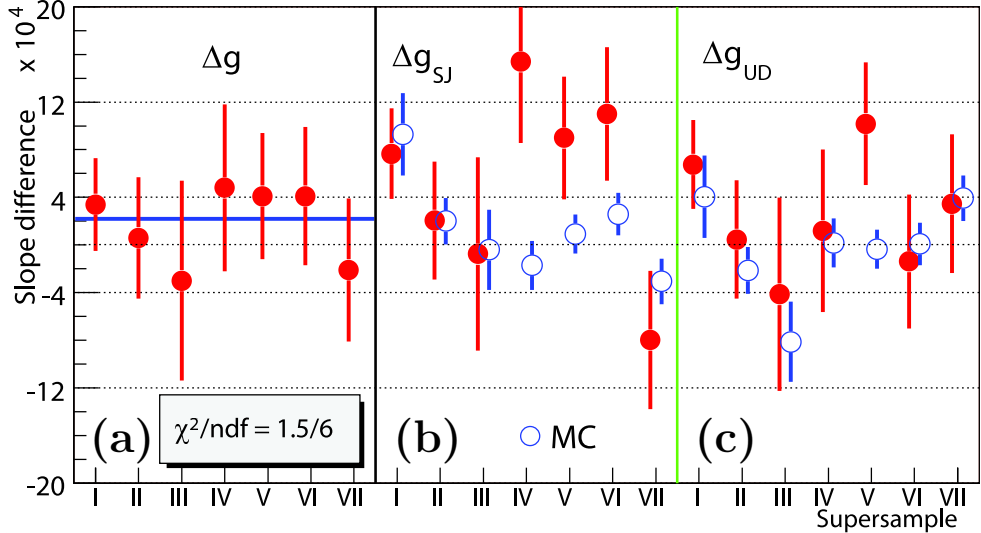


Figure 9: (a) Δg^n measurement in the seven supersamples; control quantities (b) Δg_{SJ}^n and (c) Δg_{UD}^n corresponding to detector and beam line asymmetries which cancel in quadruple ratio, and their comparison to MC.

706 cut. In particular, systematic effects due to spectrometer misalignment (see Section 3.2),
 707 momentum scale (see Section 3.3), and geometrical acceptance for the charged track (see
 708 Section 3.4), which are important issues for the analysis in the $K^\pm \rightarrow 3\pi^\pm$ mode, were
 709 found to be negligible for the $K^\pm \rightarrow \pi^\pm\pi^0\pi^0$ analysis.

710 Uncertainties related to imperfect knowledge of the permanent magnetic field in the
 711 decay volume were found not to exceed $\delta(\Delta g^n) = 0.1 \times 10^{-4}$ by artificially varying the
 712 field map in accordance with the precision of its measurement. Stability of the result with
 713 respect to variation of the selected $\pi^\pm\pi^0\pi^0$ invariant mass interval was checked, and no
 714 systematic deviation was found.

715 Systematic uncertainty due to the difference of K^+ and K^- production spectra was
 716 conservatively estimated in the same way as for the $K^\pm \rightarrow \pi^\pm\pi^+\pi^-$ mode (described in
 717 Section 3.7), and found to be $\delta(\Delta g^n) = 0.3 \times 10^{-4}$.

718 Systematic uncertainties due to event pile-up were found not to exceed $\delta(\Delta g^n) =$
 719 0.2×10^{-4} by varying the selection conditions on the allowed extra activity in the detectors,
 720 and by checking the stability of the result with respect to the timing cuts.

721 Charge-asymmetric material effects, which are negligible, were discussed in Section 3.7.

722 4.6 The resulting A_g^n

723 The systematic uncertainties are summarized in Table 6. The difference in the linear slope
 724 parameters of K^+ and K^- decays into $\pi^\pm\pi^0\pi^0$ was measured with the full NA48/2 data
 725 sample of 9.13×10^7 events to be

$$\Delta g^n = (2.2 \pm 2.1_{stat.} \pm 0.7_{syst.}) \times 10^{-4}. \quad (11)$$

726 The corresponding direct CP violating asymmetry (3) obtained using the nominal value
 727 of the linear slope parameter $g^n = 0.626 \pm 0.007$ [7] is

$$A_g^n = (1.8 \pm 1.7_{stat.} \pm 0.6_{syst.}) \times 10^{-4} = (1.8 \pm 1.8) \times 10^{-4}. \quad (12)$$

Table 6: Systematic uncertainties on the measured value of Δg^n .

Systematic effect	Uncertainty $\delta(\Delta g^n) \times 10^4$
Overlap of LKr showers	± 0.5
L1 HOD trigger inefficiency	± 0.1
L1 LKr trigger inefficiency	± 0.1
L2 trigger inefficiency	± 0.3
Stray magnetic fields	± 0.1
Kaon production spectra	± 0.3
Pile-up	± 0.2
Total systematic uncertainty	± 0.7

728 The uncertainties of the measured A_g^c and A_g^n are similar, despite a ratio of the sample
729 sizes of $N^c/N^n = 34$. The main reason for compensation of the difference in sample sizes
730 is a small ratio of the linear slope parameters of the two decay modes: $|g^c/g^n| = 0.34$.

731 5 Discussion of the results

732 The measurement of Δg differences between the linear Dalitz plot slopes was chosen as
733 a representative quantity of a possible direct CP violation effect, and is the quantity
734 on which most theoretical and experimental investigations are focused. In absence of a
735 specific model for physics beyond the SM it is not possible to state in general terms which
736 difference in K^+ and K^- decay distributions is expected to give the most significant CP
737 violating effect.

738 Discussing the asymmetry of linear slopes, it should be remarked that the recent dis-
739 covery by NA48/2 [29] (and theoretical interpretation [8, 9, 10]) of the distortion of the
740 $\pi^\pm\pi^0\pi^0$ Dalitz plot distribution due to final state interactions between pions indicated the
741 need for alternative parameterizations. Rescattering terms can be conveniently accommo-
742 dated into a parameterization based on a polynomial expansion of the decay amplitude
743 itself (rather than the event density) which, for the non-rescattering part, would be:

$$|M'(u, v)|^2 \sim (1 + g'u/2 + h'u^2/2 + k'v^2/2 + \dots)^2. \quad (13)$$

744 The relation between the slope parameters appearing in (1) and (13) is, at first order, $g' =$
745 g , $h' = h - g^2/4$, $k' = k$. Measurement of $\Delta g'$ in the framework of the parameterization
746 (13) involves fitting of the quadruple ratio of measured u distributions (5) with a function

$$f'(u) = n \cdot \left(1 + \frac{\frac{1}{2}\Delta g'u}{1 + \frac{1}{2}g'u + \frac{1}{2}h'u^2} \right)^8, \quad (14)$$

747 rather than (6).

748 The results of the measurement of Δg in the framework of parameterizations (1) and
749 (13) were compared. The result in the $K^\pm \rightarrow 3\pi^\pm$ mode is stable within 0.1×10^{-4} ,
750 and its error is insensitive to the parameterization. On the other hand, the result in the
751 $K^\pm \rightarrow \pi^\pm\pi^0\pi^0$ mode obtained with (13) is

$$\Delta g' = (3.2 \pm 3.1_{stat.}) \times 10^{-4}, \quad (15)$$

752 to be compared with (11). The significant variation of the central value and its error is
 753 mostly due to the relatively large values of the slope parameters g^n and h^n . Introduction
 754 of the additional $\pi\pi$ rescattering term to the amplitude (13) does not considerably change
 755 the result with respect to (15).

756 The sensitivity discussed above is one of the reasons to publish the tabulated quadruple
 757 ratios along with the results of the fits.

758 Conclusions

759 NA48/2 has measured the charge asymmetries of Dalitz plot linear slopes in both three-
 760 pion K^\pm decay modes to be

$$A_g^c = (-1.5 \pm 2.2) \times 10^{-4}, \quad A_g^n = (1.8 \pm 1.8) \times 10^{-4}, \quad (16)$$

761 which is an improvement in accuracy over the previous measurements [7] by more than
 762 one order of magnitude. NA48/2 precisions are limited mainly by the available statistics.

763 The measured asymmetries do not show evidences for large enhancements due to
 764 non-SM physics. They are consistent with the SM predictions, in particular with a full
 765 next-to-leading order ChPT calculation [12] predicting

$$A_g^c = (-1.4 \pm 1.2) \times 10^{-5}, \quad A_g^n = (1.1 \pm 0.7) \times 10^{-5}. \quad (17)$$

766 Due to the high precision achieved, the results can be used to constrain extensions of the
 767 SM predicting enhancements of the CP violating effects.

768 Acknowledgements

769 It is a pleasure to thank the technical staff of the participating laboratories, universi-
 770 ties and affiliated computing centres for their efforts in the construction of the NA48
 771 apparatus, in the operation of the experiment, and in the data processing.

References

- [1] J.H. Christenson *et al.*, Phys. Rev. Lett. **13** (1964) 138.
- [2] H. Burkhardt *et al.* (NA31), Phys. Lett. **B206** (1988) 169.
 G. Barr *et al.* (NA31), Phys. Lett. **B317** (1993) 233.
- [3] V. Fanti *et al.* (NA48), Phys. Lett. **B465** (1999) 335.
 A. Lai *et al.* (NA48), Eur. Phys. J. **C22** (2001) 231.
 J.R. Batley *et al.* (NA48), Phys. Lett. **B544** (2002) 97.
- [4] A. Alavi-Harati *et al.* (KTeV), Phys. Rev. Lett. **83** (1999) 22.
 A. Alavi-Harati *et al.* (KTeV), Phys. Rev. **D67** (2003) 012005.
- [5] B. Aubert *et al.* (Babar), Phys. Rev. Lett. **87** (2001) 091801.
 K. Abe *et al.* (Belle), Phys. Rev. Lett. **87** (2001) 091802.

- [6] K. Abe *et al.* (Belle), Phys. Rev. Lett. **93** (2004) 021601.
B. Aubert *et al.* (Babar), Phys. Rev. Lett. **93** (2004) 131801.
- [7] W.-M. Yao *et al.* (PDG), J. Phys. **G33** (2006) 1.
- [8] N. Cabibbo, Phys. Rev. Lett. **93** (2004) 121801.
- [9] N. Cabibbo and G. Isidori, JHEP **0503** (2005) 021.
- [10] G. Colangelo *et al.*, Phys. Lett. **B638** (2006) 187.
- [11] G. Isidori, L. Maiani, A. Pugliese, Nucl. Phys. **B381** (1992) 522.
- [12] E. Gámiz, J. Prades, I. Scimemi, JHEP **10** (2003) 042.
- [13] G. Fäldt, E. Shabalin, Phys. Lett. **B635** (2006) 295.
- [14] E.P. Shabalin, ITEP preprint **8-98** (1998).
G. D'Ambrosio, G. Isidori, G. Martinelli, Phys. Lett. **B480** (2000) 164.
- [15] W.T. Ford *et al.*, Phys. Rev. Lett. **25** (1970) 1370.
- [16] K.M. Smith *et al.*, Nucl. Phys. **B91** (1975) 45.
G.A. Akopdzhanov *et al.* (TNF-IHEP), Eur. Phys. J. **C40** (2005) 343.
- [17] J.R. Batley *et al.* (NA48/2), Phys. Lett. **B634** (2006) 474.
- [18] J.R. Batley *et al.* (NA48/2), Phys. Lett. **B638** (2006) 22.
- [19] Y. Giomataris *et al.*, Nucl. Inst. Methods **A376** (1996) 29.
- [20] B. Peyaud *et al.*, Nucl. Inst. Methods **A535** (2004) 247.
- [21] D. Bèderède *et al.*, Nucl. Inst. Methods **A367** (1995) 88.
- [22] G.D. Barr *et al.*, Nucl. Inst. Methods **A370** (1996) 413.
- [23] V. Fanti *et al.* (NA48), Nucl. Inst. Methods **A574** (2007) 433.
- [24] J.R. Batley *et al.* (NA48/2), Phys. Lett. **B649** (2007) 349.
- [25] GEANT Description and Simulation Tool, CERN Program Library Long Writeup **W5013** (1994).
- [26] R. Frühwirth, Nucl. Inst. Methods **A262** (1987) 444.
- [27] J.R. Cudell *et al.*, Phys. Rev. **D65** (2002) 074024.
- [28] H.W. Atherton *et al.*, CERN 80-07.
- [29] J.R. Batley *et al.* (NA48/2), Phys. Lett. **B633** (2006) 173.